8-21-2018

Electrospray Ionization of Polypropylene Glycol: Rayleigh-Charged Droplets, Competing Pathways, and Charge State-Dependent Conformations.

Quentin Duez

Haidy Metwally

Lars Konermann

Electrospray Ionization of Polypropylene Glycol: Rayleigh-Charged Droplets, Competing Pathways, and Charge State-Dependent Conformations

Quentin Duez[1,2], Haidy Metwally[1], and Lars Konermann[1,*]

[1]*Department of Chemistry, The University of Western Ontario, London, Ontario, N6A 5B7, Canada.*

[2]*Organic Synthesis and Mass Spectrometry Laboratory, University of Mons, Place du Parc, 23, Mons, 7000, Belgium*

* corresponding author: konerman@uwo.ca

Funding was provided by the Natural Sciences and Engineering Research Council of Canada RGPIN-2018-04243). QD was recipient of travel stipends from the Belgian Fonds National de la Recherche Scientifique, Université de Mons, and the Académie des Sciences and Faculté Wallonie-Bruxelles.

ABSTRACT: Recent molecular dynamics (MD) simulations from various laboratories have advanced the general understanding of electrospray ionization (ESI)-related processes. Unfortunately, computational cost has limited most of those previous endeavors to ESI droplets with radii of ~3 nm or less, which represent the low end of the size distribution in the ESI plume. The current work extends this range by conducting simulations on aqueous ESI droplets with radii of 5.5 nm (~23000 water molecules). Considering that computational cost increases with r^6, this is a significant step forward. We focused on the ESI process for polypropylene glycol (PPG) which is a common ESI-MS calibrant. Different chain lengths (PPG10, 30, and 60) were tested in droplets that were charged with excess Na^+. Solvent evaporation and Na^+ ejection, with occasional progeny droplet formation, kept the systems at 80-100% of the Rayleigh limit throughout their life cycle. PPG chains migrated to the droplet surface where they captured Na^+ via binding to ether oxygens. Various possible pathways for PPG release into the gas phase were encountered. Some PPG10 runs showed ejection from the droplet surface, consistent with the ion evaporation model (IEM). In other instances, PPG was released after near-complete solvent evaporation, as envisioned by the charged residue model (CRM). A third avenue was the partial separation from the droplet to form double or single-tailed structures, with subsequent chain detachment from the droplet. This last pathway is consistent with the chain ejection model (CEM). Immediately after detachment many chains were electrostatically stretched, but they subsequently collapsed into compact conformers. Extended structures were retained only for the most highly charged ions. Our simulations were complemented by ESI-MS and ion mobility measurements. MD-predicted charge states and collision cross sections were in agreement with these experimental data, supporting the mechanistic insights obtained.

Synthetic polymers affect all aspects of our daily lives. Electrospray ionization (ESI)[1] and matrix-assisted laser desorption/ionization (MALDI)[2] mass spectrometry (MS) have become key tools for the characterization of these analytes.[3-6] ESI-MS is commonly used for studying polymers that are soluble in organic, aqueous, or mixed solvent systems.[7, 8] Many of these investigations have benefited from the incorporation of ion mobility spectrometry (IMS) for ESI-IMS/MS workflows.[9, 10]

The question how gaseous analyte ions are produced during the ESI process has captivated the analytical research community for decades.[11-20] An ESI emitter produces charged droplets that undergo evaporation and Coulombic fission. These processes ultimately generate nanodroplets from which ions are released into the gas phase.[11] Early evaporation/fission events in the ESI plume can be examined by imaging,[21-23] phase Doppler anemometry,[24] and levitation studies.[25, 26] The final nanodroplets are much more difficult to examine because of their heterogeneity, short lifetimes, and small size. As a result, the mechanisms of analyte ion release from ESI nanodroplets remain controversial.[11-20] One classical scenario is the ion evaporation model (IEM), which envisions that analytes undergo field emission from the droplet surface.[27, 28] Alternatively, the charged residue model (CRM) refers to conditions where analyte ions are liberated by droplet evaporation to dryness.[13] It is often assumed that the IEM applies to small pre-charged analytes, whereas the CRM is operative for large globular species.[11, 13] However, this distinction is not universally accepted. For example, Fenn promoted the view that the IEM is operative from small ions to large synthetic macromolecules such as polyethylene glycol (PEG).[1]

Molecular dynamics (MD) simulations have become an important tool for ESI mechanistic investigations.[29-37] Several MD studies demonstrated the ejection of small ions from charged nanodroplets, consistent with the IEM.[20, 29-31] Simulations on peptides,[37] native proteins,[32] and nucleic acids [33] indicated that these larger species follow the CRM.

A general challenge associated with ESI simulations is the droplet size. The ESI plume comprises droplets with radii as large as micrometers, all the way down to 2-3 nm.[11, 21, 22] To keep simulation times manageable, previous MD studies mostly focused on small droplets with radii on the order of 3 nm or less, corresponding to a few thousand solvent molecules.[20, 29-33, 35-37] The droplet size in those earlier studies was typically chosen just large enough to ensure a few solvent layers between the analyte and the droplet surface at the onset of the simulation. MD investigations on larger droplets would provide a more comprehensive view of the events in the ESI plume. Unfortunately, such endeavors are associated with high computational cost which scales as N^2 with the number of atoms N, implying a staggering r^6 scaling with droplet radius r.[38]

PEG has served as a model compound in a number of ESI mechanistic studies.[35, 36, 39-43] In positive ion mode, PEG produces cationized ions such as $[PEG + zNa^+]^{z+}$ that have their charge carriers bound via ether oxygens.[34] Consta *et al*. pioneered the use of MD simulations for PEG-containing aqueous droplets.[35, 36] Those simulations revealed that PEG partitions to the droplet surface. Na^+ binding with subsequent separation of one chain end from the surface then produces droplets with dangling polymer tails. These PEG chains can detach, or the droplets can dry out without PEG detachment. Our laboratory proposed that a similar ESI mechanism applies to unfolded proteins, i.e., gradual expulsion of the unfolded chain to generate tadpole-shaped intermediates, followed by protein detachment from the droplet.[20] For proteins, this chain ejection model (CEM)[20, 44] involves the equilibration of mobile protons between the droplet and the protruding chain,[20] resembling the behavior of collisionally activated multi-subunit complexes.[45-47]

In contrast to PEG,[35, 36, 39-43] polypropylene glycol (PPG) has received very little attention from an ESI mechanistic perspective. This is despite the fact that PPG is of greater practical importance for many ESI-MS experimentalists who use it as mass calibrant, often relying on commercial pre-mixed standards.[48-50] PPG charging takes place via cationization with Na^+ or other

small ions. Similar to PEG, PPG binds these charge carriers with its ether oxygens, giving rise to charge-solvated $[PPG + zNa^+]^{z+}$ gas phase species.[34, 51]

In this work we conducted comprehensive ESI-IMS/MS experiments and MD simulations to elucidate the mechanism by which gaseous $[PPG + zNa^+]^{z+}$ ions are produced from aqueous ESI droplets. We extended the droplet size in our MD runs to ~23000 water molecules (radius 5.5 nm), which are the largest simulated ESI droplets to date. This advance was facilitated by graphics processing unit (GPU)-accelerated computing which provides a major performance boost.[52] The data obtained were compared with simulations on smaller (3 nm) droplets which represent a size regime comparable to that used in earlier MD studies on other analytes.[20, 29-33, 35-37] We also subjected the liberated PPG ions to long (1 μs) vacuum simulations to capture their post-ESI behavior. Simulation data produced in this way were in excellent agreement with experimental charge states and collision cross sections, providing the first detailed view of the PPG journey from solution into the vacuum of the mass spectrometer.

Materials and Methods

ESI-MS and Ion Mobility Measurements. Mass spectra were acquired on a Synapt HDMS instrument (Waters, Milford, MA). 50 μM PPG samples with nominal average mass values of 400 Da, 1200 Da, 2000 Da, and 2700 Da (Sigma, St. Louis, MO) were electrosprayed at 1.3 kV using gold-coated borosilicate nanoESI emitters, a cone voltage 30 V, and at a source temperature 80° C. The solutions contained 250 μM sodium acetate. Initial test experiments in pure aqueous solution provided unstable spray conditions, this problem was remedied by the addition of 5% v/v acetonitrile. Collision cross sections Ω_{exp} were measured using the traveling wave ion mobility cell

of the Synapt (IMS wave height 9 V, wave velocity 450 m^{-1}, N_2 flow rate 14 mL min^{-1}).[53] Ω_{exp} values are reported as effective He collision cross sections, calibrated as described.[54]

MD Simulations were conducted using Gromacs[55] 2016 with GPU acceleration[52] and the Charmm36 force field.[56] TIP4P/2005 water was chosen because it matches the experimental water surface tension (0.05891 N m^{-1} at 370 K), while other models yield lower values.[57] Materials Studio (BIOVIA, San Diego, CA) was used to generate initial PPG coordinate files. Topologies were obtained using the ParamChem Server.[58] Neutral PPG was initially equilibrated without solvent for 100 ns at 600 K, followed by 10 ns at 298 K. Random frames from the 298 K runs served as starting points for subsequent ESI simulations. Spherical droplets with 5.5 nm radius (~23000 H_2O molecules) or 3.0 nm radius (~3500 H_2O) were built around the chains. For the larger droplets 47 Na^+ were placed in random positions, while for the smaller droplets 19 Na^+ were used. The droplet charge under these initial conditions is close to the Rayleigh limit.[11] ESI droplet simulations were conducted in vacuum using a trajectory stitching approach with 250 ps run segments at 370 K for a total of 75 ns.[32] For each chain length we generated three replicate 5.5 nm droplet runs with different initial PPG conformations and velocities. For the smaller droplets five replicates were generated. The droplet simulations were followed by 1 μs vacuum runs in the absence of water, using the simulated ESI products as starting structures. He collision cross sections Ω_{calc} of PPG ions were calculated using the trajectory method[59] in Collidoscope.[60] Atomic coordinates and charges for Collidoscope were taken from Gromacs .gro and .itp files, respectively. Ω_{calc} values were determined by extracting 11 MD structures from the 1 μs vacuum trajectories in 50 ns intervals, starting at t = 500 ns.

Results and Discussion

ESI Mass Spectra. PPG mass spectra showed wide $[PPG + zNa^+]^{z+}$ peak distributions that reflect the polydisperse nature of the samples. Figure 1 exemplifies the spectrum of PPG with a nominal average MW of 2000 Da. Three groups of peaks are discernible, corresponding to 1+, 2+, and 3+ ions. It is difficult to gauge the actual abundances of differently charged ions from the peak intensities, because the spectra will be skewed by *m/z*-dependent differences in transmission and/or detection efficiency.[61] In Figure 1 the highest intensity signals correspond to PPG28 for 1+, PPG31 for 2+, and PPG34 for 3+. Considering that the 1+/2+/3+ ions all originate from the same analyte mass distribution, the trend implies that high *m/z* ions were transmitted and/or detected less efficiently. In other words, the actual abundance of 1+ PPG ions in the ESI plume was likely much higher than suggested by the peak intensities in Figure 1. This assertion is consistent with the transmission properties of RF ion guides and ESI ion sampling interfaces,[61] although the situation may be further complicated by MW-dependent changes in cationization efficiency.[62]

The aqueous solutions in our experiments contained a small fraction (5%) of acetonitrile which enhanced signal stability, likely by aiding liquid dispersion at the Taylor cone.[11, 22] Organic cosolvents such as acetonitrile undergo preferential evaporation,[63, 64] implying that late ESI nanodroplets under the conditions of our work will be predominantly aqueous.[69, 70] For this reason the MD simulations discussed below focused on aqueous droplets without acetonitrile. Na^+ served as charge carrier, reflecting the presence of sodium ions in the experimental solutions. The simulations focused on three specific chain lengths, i.e., H-[O-CH(CH_3)-CH_2]$_n$-OH with n = 10, 30, and 60, referred to as PPG10, PPG30, and PPG60. The experimental mass spectra revealed that PPG10 exclusively formed 1+ ions. In the case of PPG30 we observed charge states 1+, 2+, and 3+, while PPG60 formed 2+, 3+, and 4+ ions.

5.5 nm Droplet Simulations. Snapshots taken from typical ESI simulations on PPG-containing aqueous droplets with an initial radius of 5.5 nm are shown in Figure 2. While the droplets shrunk due to water evaporation, the PPG molecules migrated to the surface within ~20 ns and remained surface-associated for another 10-20 ns. After reaching the surface, many of the chains captured one or more Na^+ ions from the solvent via electrostatic interactions with their ether oxygens. For PPG10 these charge capture events were soon followed by electrostatically driven detachment of the entire chain from the droplet (Figure 2a, 26.4 ns). For PPG30 and PPG60 the capture of one or two Na^+ initially triggered partial separation from the droplet, producing tadpole-like structures (Figure 2b, 41.3 ns; Figure 2c, 37.5 ns). The polymer tails of the droplets adopted stretched-out conformations due to Coulombic repulsion between the PPG-associated Na^+ and the charged droplet. In some cases this electrostatic force was sufficient to trigger polymer detachment from droplet after binding of only one Na^+ (Figure 2b, 41.4 ns). In other runs complete separation of the polymer from the droplet occurred after binding of additional Na^+ (Figure 2c, 46.48 ns).

Immediately after detaching from the droplet the PPG chains retained water molecules around their bound Na^+. This residual water subsequently evaporated, sometimes in conjunction with loss of a hydrated Na^+. One of these charge loss incidents is exemplified in Figure 2c, where PPG60 was ejected as hydrated 3+ ion, while ultimately only two Na^+ remained attached. None of the runs showed Na^+ loss from a dry PPG ion, implying that electrostatic screening by H_2O is a prerequisite for these charge loss events.

Coulombic destabilization of ESI droplets facilitates events that would not be feasible for neutral systems, such as the expulsion of charged PPG and the IEM ejection of Na^+ (Figure 2). In principle, the emission of charged progeny droplets is another mechanism by which the system can relieve electrostatic stress. Kinetic and energetic arguments suggest, however, that droplet fission is feasible only for relatively large droplets, not for those with radii of 2-3 nm.[11, 27] Consistent with

this expectation,[11, 27] previous simulations on aqueous nanodroplets (with typical radii ≤ 3 nm) did not show progeny droplet formation. The situation is different in some of the 5.5 nm droplets runs examined here. Figure 3a illustrates the ejection of a cluster containing ~120 H_2O and 2 Na^+. The size of the ejected cluster and the fact that it contains more than one Na^+ implies that this is *not* a typical IEM event.[20, 27-31] Instead, the morphology of the process closely resembles droplet fission detected in imaging experiments on larger droplets.[11, 21, 22] In other words, Figure 3a reveals that for radii around 5.5 nm droplet fission starts to become a viable alternative to IEM and analyte ejection events. Fission processes for even larger droplets have been studied previously using simplified continuum models,[23, 65] but not in atomistic MD simulations.

The data of Figure 3a are also interesting from another perspective. PPG10 migrated to the surface of the 5.5 nm droplet within ~20 ns. One possible outcome under these conditions is Na^+ binding with subsequent PPG detachment from the droplet (as in Figure 2a). In Figure 3a, however, the system followed a different pathway. PPG10 stayed at the surface while the droplet evaporated to dryness. Binding of the last remaining Na^+ to PPG10 produced a gaseous "charged residue". By definition, formation of gaseous $[PPG10 + Na]^+$ in Figure 3a thus represents a CRM process. This is in contrast to the runs discussed earlier, which displayed IEM behavior (for PPG10, Figure 2a) or CEM behavior (for PPG30 and PPG60, Figure 2a, b). In other words, our data reveal a range of possible scenarios for the production of gaseous PPG ions from aqueous ESI droplets.

3 nm Droplet Simulations. Diverse ESI scenarios were also observed in simulations on droplets with initial radii of 3 nm. PPG migration to the surface of these smaller droplets occurred within ~1 ns, exemplified in Figure 3b for PPG60. In this particular trajectory one end of the charged chain initially separated from the droplet. This was followed by sodiation and separation of the other chain end, producing a double-tailed intermediate that persisted for ~20 ns. Ultimately, the

center section of the chain detached from the droplet, producing a 4+ ion. Double-tailed intermediates were observed in two (out of five) 3 nm PPG60 runs, but not under any other conditions. Additional simulations on PPG10, PPG30, and PPG60 displayed various other scenarios (Figure S2). In most runs the polymer detached from the surface in a CEM-like fashion, after the formation of single-tail intermediates (Figure S2a). In several instances detachment took place only after the droplet had evaporated to a small fraction of its initial size (Figure S2b). In other runs the polymer did not detach from the droplet, but instead the whole system gradually dried out (CRM behavior, Figure S2c). Droplet fission was not observed for the 3 nm droplets.

Droplet Evaporation Close to the Rayleigh Limit. Evaporative droplet shrinkage was accompanied by the ejection of solvated Na^+ from the droplet, exemplified in the top right panel of Figure 2 (see also Figure S1). Such charge ejection events follow the IEM.[20, 27-31] The number of charges on the droplet (z_D) can be expressed relative to the Rayleigh charge (z_R) according to[11]

$$z_D/z_R = z_D \times \left(\frac{8\pi}{e}\sqrt{\varepsilon_0\,\gamma\,r^3}\right)^{-1} \qquad (1)$$

with the vacuum permittivity ε_0, the surface tension γ, and the elementary charge e. It is instructive to examine how z_D/z_R depends on the number of water molecules n_{water}. Assuming that the aqueous droplet is spherical, n_{water} can be estimated[13] using (*mass*) = (*density* × *volume*) as

$$\left(n_{water} \times \frac{0.001\times 18.02}{6.02\times 10^{23}}\right)\ \text{kg} = \left(1000\ \times \frac{4}{3}\pi\, r^3\right)\ \text{kg} \qquad (2)$$

By substituting r^3 from eq 2 into eq 1 we obtain an expression for z_D/z_R as a function of n_{water}. The droplet charge can only adopt discrete values, giving rise to multiple possible z_D/z_R vs. n_{water} plots (gray lines in Figure 4 for z_D = ... 6+, 7+, 8+ ...). Any droplet consisting of n_{water} molecules with an arbitrary charge z_D will fall on one of these lines. For the PPG-containing droplets considered here the assumption of a purely aqueous system will break down at some point, which is why the plots of Figure 4 were arbitrarily truncated at n_{water} = 1000.

Like most previous ESI modeling studies[29-37] our simulations employed a manually selected initial charge of $z_D/z_R \approx 1$, reflecting the view that droplets in the ESI plume are close to the Rayleigh limit.[11, 13, 24] During the MD runs the droplets showed sawtooth-like z_D/z_R patterns, (Figure 4). These patterns arose from solvent evaporation which gradually increased the charge density along one of the predefined grey z_D/z_R lines, until an IEM event caused a downward jump to the adjacent $(z_D - 1)/z_R$ line. These alternating processes kept the systems within a relatively narrow z_D/z_R range between 0.8 and 1.0 (Figure 4).

Sawtooth data of the type shown in Figure 4a have been discussed previously for 3 nm droplets,[32] and it was noted that the simulated patterns resemble experimental z_D/z_R profiles observed for much larger (μm) droplets.[24] Critics might argue that the evolution of simulated droplets close to the Rayleigh limit through a few evaporation/IEM cycles (6-8 in Figure 4a) could be a short-term memory effect that echoes the manually selected $z_D/z_R \approx 1$ initial condition. Simulations on larger droplets can address this concern. The z_D/z_R profiles of 5.5 nm droplet runs displayed a much greater number of evaporation/IEM cycles with occasional progeny droplet emission (~30 cycles, Figure 4b). Also in the case of these larger droplets, z_D/z_R oscillated in the range of 0.8 to 1.0 with a slightly increasing amplitude towards the end of the process. Once the 5.5 nm droplets had shrunk to around 3 nm (Figure 4b), their z_D/z_R profiles were virtually indistinguishable from those of the 3 nm droplets (Figure 4a). These findings imply that the

evaporation of ESI droplets takes place in a range of $0.8 \leq z_D/z_R \leq 1$ regardless of droplet size. We conclude that MD-simulated evaporation close to the Rayleigh limit is *not* a computational fluke that only applies to very small nanodroplets. Instead, the condition $0.8 \leq z_D/z_R \leq 1$ represents an intrinsic property of Na^+-containing aqueous ESI droplets.[11, 13, 24] In the subsequent section we will discuss that, despite their similar z_D/z_R profiles, 5.5 nm and 3 nm droplets nonetheless show some differences regarding the charge states of their released PPG ions.

Charge States. Figure 5 summarizes the MD results for 5.5 nm and 3 nm droplets, providing information on evaporation kinetics, ESI scenarios, and PPG charge states. 15 out of 24 runs culminated in the detachment of sodiated PPG from the droplet surface (CEM or IEM events). In the remaining runs PPG ions were formed via solvent evaporation to dryness, or by detaching from droplets that had undergone almost complete evaporation to $n_{water} < 300$ (CRM-like events).

The range of MD-generated charge states showed excellent agreement with the experimental values. PPG10 simulations and experiments solely produced 1+ ions. Similarly, for PPG30 the MD-predicted range of 1+ to 3+ agreed with the experimental mass spectra (Figure 1). Experimental PPG60 spectra covered the charge states 2+ to 4+, all of which were also produced in simulations. Only one PPG60 simulation fell outside the experimentally observed range (5+, Figure S2c). Interestingly, neither the 5.5 nm nor the 3 nm droplet runs *alone* could account for the complete range of experimentally observed charge states. For PPG60, in particular, both simulated droplet sized were required to match the ESI-MS data. This behavior suggests that under experimental conditions droplets of various sizes contribute to the formation of gaseous analyte ions, including the 3 nm to 5.5 nm range studied in our simulations. The involvement of various droplet sizes is consistent with the known heterogeneous droplet size distribution within the ESI

plume.[11, 21, 22, 24] Clearly, we cannot rule out that droplets outside of the size range studied here also contribute to the production of PPG ions.

The 5.5 nm droplet simulations on PPG30 and PPG60 produced somewhat lower charge states than the 3 nm droplet runs (Figures 5b/5e, and 5c/5f). This difference likely originates from the fact that PPG detachment from the 5.5 nm droplets preferentially took place at an earlier stage of the evaporation process (with n_{water} in the range of 2000 to 4000, Figure 5b-c). In contrast, for the 3 nm runs most detachment events took place for $n_{water} < 1000$ (Figure 5e-f). PPG detachment from the smaller droplets was preceded by structures where the chain was wrapped around a significant portion of the droplet (Figure 3b). Such close chain/droplet contacts favored Na^+ binding to the PPG chains, thereby promoting the formation of slightly higher charge states.

Gas Phase Structures. Ω_{exp} values obtained from IMS experiments increased in the order PPG10 < PPG30 < PPG60 (Figure 6). In addition, the Ω_{exp} values of PPG30 (Figure 6b-d) and PPG60 (Figure 6e-g) increased with increasing charge state. The latter trend arises from internal charge repulsion which favors expanded conformers, similar to the behavior of gaseous proteins.[66, 67]

Our simulations revealed that most PPG chains emerged from the droplet via tadpole-like intermediates (CEM), where electrostatic droplet/chain repulsion stretched the polymer tails into extended conformations. These stretched conformations persisted until right after detachment from the droplet (e.g., Figure 2b at 41.4 ns, and Figure 2c for 46.48 ns). Subsequently many of the chains collapsed into more compact structures (final frames in Figures 2b, 2c, S2a). Extended conformations after detachment were preserved only for the highest charge states such as $[PPG60 + 4Na]^{4+}$ (final frame of Figure 3b). To examine the long-term behavior of PPG after release into the gas phase we performed 1 μs vacuum simulations on the ESI products. Representative structures obtained in this way are included in Figure 6. $[PPG10 + Na]^+$, $[PPG30 + 2Na]^{2+}$, and

$[PPG60 + 2Na]^{2+}$ adopted compact structures with buried charge-solvated Na^+ ions (Figure 6a, b, e). The addition of subsequent Na^+ produced less compact conformers (Figure 6c, f). The highest charge states $[PPG30 + 3Na]^{3+}$, and $[PPG60 + 4Na]^{4+}$ retained extended structures, with small loops that accommodated each Na^+ via interactions with ~6 ether oxygens. The Ω_{exp} distribution of $[PPG60 + 4Na]^{4+}$ was relatively wide, suggesting that structural heterogeneity for this ion type was more pronounced than expected (Figure 6g). Overall, Figure 6 reveals that all of the MD-predicted charge state and size trends on PPG collision cross sections were confirmed experimentally. Most of the Ω_{calc} values were gratifyingly close to the corresponding Ω_{exp} distributions (Figure 6, red lines and black profiles).

Conclusions

Focusing on PPG, the current work tracked the transformation of synthetic polymers from droplet-dissolved species into structurally equilibrated gas phase ions. Our MD runs employed the largest aqueous ESI droplets simulated to date, with radii of 5.5 nm. Consistent with theoretical predictions,[11, 27] for this droplet size range the formation of progeny droplets starts to compete with other charge loss processes. The main pathway by which the shrinking ESI droplets shed charge, however, remains the IEM ejection of solvated charge carriers (Na^+ for the droplets studied here). These IEM events keep the system at 80% to 100% of the Rayleigh limit throughout the droplet life cycle. Thus, regardless of the mechanism by which analyte molecules ultimately get transformed into gaseous ions, the IEM plays an ancillary role during the ESI process.

Our simulations revealed that PPG gas phase ions can form via different pathways. Cationized PPG10 can eject from the surface of large droplets (consistent with the IEM), while in

other runs the droplet almost completely dried out before the analyte was released (a CRM-like feature). Many runs for longer chains showed CEM-like behavior, where the chain detached from the droplet after formation of tadpole-shaped intermediates with long polymer tails. Both one- and two-tailed structures were observed. In contrast to the CEM mechanism proposed for proteins,[20] the CEM pathway for PPG does not include the migration of mobile H^+ along the chain. Instead, PPG-associated Na^+ were able to undergo only minor positional arrangements as long as they were surrounded by residual water. After desolvation the positions of oxygen-linked Na^+ were fixed. Even for PPG30 and PPG60 we observed instances where the polymer chains were released into the gas phase following CRM-like scenarios, with near-complete solvent evaporation. This multitude of possible ESI scenarios goes well beyond the "black and white" IEM vs. CRM disputes in the older literature.[1, 11-15, 27, 28] Our work demonstrates that there are many shades of gray. The appropriateness of our simulation strategy is supported by the fact that it predicts experimental PPG charge states and gas phase conformations remarkably well.

With ongoing improvements in computer hardware and simulation software it may soon be possible to extend the size range of ESI simulations to even larger droplets. Such endeavors would provide additional details of the evaporation and fission events within the ESI plume. Also, it should be possible to further scrutinize the relationship between droplet size and IEM/CRM/CEM events, possibly extending to ESI avenues that yet remain to be discovered. MD methods hold enormous promise for understanding the physical basis of chemical analysis methods. It is hoped that the current study will promote the widespread acceptance of this computational approach by the analytical community.

Supporting Information Available. Additional figures as noted in the text. This material is available free of charge via the Internet at http://pubs.acs.org.

References

(1) Nguyen, S.; Fenn, J. B. *Proc. Natl. Acad. Sci. U.S.A.* **2007**, *104*, 1111-1117.
(2) Karas, M.; Hillenkamp, F. *Anal. Chem.* **1988**, *60*, 2299-2301.
(3) Hanton, S. D. *Chem. Rev.* **2001**, *101*, 527-569.
(4) McEwen, C. N.; Peacock, P. M. *Anal. Chem.* **2002**, *74*, 2743-2748.
(5) Crecelius, A. C.; Baumgaertel, A.; Schubert, U. S. *J. Mass Spectrom.* **2009**, *44*, 1277-1286.
(6) Weidner, S. M.; Trimpin, S. *Anal. Chem.* **2010**, *82*, 4811-4829.
(7) Floris, F.; Vallotto, C.; Chiron, L.; Lynch, A. M.; Barrow, M. P.; Delsuc, M. A.; O'Connor, P. B. *Anal. Chem.* **2017**, *89*, 9892-9899.
(8) Przybylski, C.; Jarroux, N. *Anal. Chem.* **2011**, *83*, 8460-8467.
(9) Hilton, G. R.; Jackson, A. T.; Thalassinos, K.; Scrivens, J. H. *Anal. Chem.* **2008**, *80*, 9720-9725.
(10) Wesdemiotis, C. *Angew. Chem.-Int. Edit.* **2017**, *56*, 1452-1464.
(11) Kebarle, P.; Verkerk, U. H. *Mass Spectrom. Rev.* **2009**, *28*, 898-917.
(12) Cole, R. B. *J. Mass. Spectrom.* **2000**, *35*, 763-772.
(13) de la Mora, F. J. *Anal. Chim. Acta* **2000**, *406*, 93-104.
(14) Cech, N. B.; Enke, C. G. *Mass Spectrom. Rev.* **2001**, *20*, 362-387.
(15) Iavarone, A. T.; Williams, E. R. *J. Am. Chem. Soc.* **2003**, *125*, 2319-2327.
(16) Hogan, C. J.; Carroll, J. A.; Rohrs, H. W.; Biswas, P.; Gross, M. L. *Anal. Chem.* **2009**, *81*, 369-377.
(17) Kaltashov, I. A.; Mohimen, A. *Anal. Chem.* **2005**, *77*, 5370-5379.
(18) Li, J.; Santambrogio, C.; Brocca, S.; Rossetti, G.; Carloni, P.; Grandori, R. *Mass Spectrom. Rev.* **2016**, *35*, 111-122.
(19) Ogorzalek Loo, R. R.; Lakshmanan, R.; Loo, J. A. *J. Am. Soc. Mass Spectrom.* **2014**, *25*, 1675-1693.
(20) Konermann, L.; Ahadi, E.; Rodriguez, A. D.; Vahidi, S. *Anal. Chem.* **2013**, *85*, 2-9.
(21) Gomez, A.; Tang, K. *Phys. Fluids* **1994**, *6*, 404-414.
(22) Nemes, P.; Marginean, I.; Vertes, A. *Anal. Chem.* **2007**, *79*, 3105-3116.
(23) Giglio, E.; Gervais, B.; Rangama, J.; Manil, B.; Huber, B. A. *Phys. Rev. E* **2008**, *77*, 036319.
(24) Grimm, R. L.; Beauchamp, J. L. *J. Phys. Chem. A* **2010**, *114*, 1411-1419.
(25) Haddrell, A. E.; Agnes, G. R. *Anal. Chem.* **2004**, *76*, 53-61.
(26) Duft, D.; Achtzehn, T.; Muller, R.; Huber, B. A.; Leisner, T. *Nature* **2003**, *421*, 128.
(27) Iribarne, J. V.; Thomson, B. A. *J. Chem. Phys.* **1976**, *64*, 2287-2294.
(28) Loscertales, I. G.; de la Mora, J. F. *J. Chem. Phys.* **1995**, *103*, 5041-5060.
(29) Higashi, H.; Tokumi, T.; Hogan, C. J.; Suda, H.; Seto, T.; Otani, Y. *Phys. Chem. Chem. Phys.* **2015**, *17*, 15746-15755.
(30) Znamenskiy, V.; Marginean, I.; Vertes, A. *J. Phys. Chem. A* **2003**, *107*, 7406-7412.
(31) Consta, S.; Mainer, K. R.; Novak, W. *J. Chem. Phys.* **2003**, *119*, 10125-10132.
(32) McAllister, R. G.; Metwally, H.; Sun, Y.; Konermann, L. *J. Am. Chem. Soc.* **2015**, *137*, 12667-12676.
(33) Porrini, M.; Rosu, F.; Rabin, C.; Darre, L.; Gomez, H.; Orozco, M.; Gabelica, V. *ACS Central Sci.* **2017**, *3*, 454–461.
(34) Gidden, J.; Wyttenbach, T.; Jackson, A. T.; Scrivens, J. H.; Bowers, M. T. *J. Am. Chem. Soc.* **2000**, *122*, 4692-4699.
(35) Chung, J. K.; Consta, S. *J. Phys. Chem. B* **2012**, *116*, 5777-5785.

(36) Oh, M. I.; Consta, S. *J. Am. Soc. Mass Spectrom.* **2017**, *28*, 2262-2279.
(37) Kim, D.; Wagner, N.; Wooding, K.; Clemmer, D. E.; Russell, D. H. *J. Am. Chem. Soc.* **2017**, *139*, 2981-2988.
(38) Caleman, C.; van der Spoel, D. *J. Chem. Phys.* **2006**, *125*, 1545081-1545089.
(39) Elliott, A. G.; Harper, C. C.; Lin, H. W.; Williams, E. R. *Analyst* **2017**, *142*, 2760-2769.
(40) Larriba, C.; de la Mora, F.; Clemmer, D. E. *J. Am. Soc. Mass Spectrom.* **2014**, *25*, 1332-1345.
(41) Ude, S.; de la Mora, J. F.; Thomson, B. A. *J. Am. Chem. Soc.* **2004**, *126*, 12184-12190.
(42) Nohmi, T.; Fenn, J. B. *J. Am. Chem. Soc.* **1992**, *114*, 3241-3246.
(43) Larriba-Andaluz, C.; Hogan, C. J. *J. Chem. Phys.* **2014**, *141*.
(44) Donor, M. T.; Ewing, S. A.; Zenaidee, M. A.; Donald, W. A.; Prell, J. S. *Anal. Chem.* **2017**, *89*, 5107-5114.
(45) Fegan, S. K.; Thachuk, M. *J. Chem. Theory Comput.* **2013**, *9*, 2531-2539.
(46) Ruotolo, B. T.; Hyung, S.-J.; Robinson, P. M.; Giles, K.; Bateman, R. H.; Robinson, C. V. *Angew. Chem. Int. Ed.* **2007**, *46*, 8001-8004.
(47) Quintyn, R. S.; Zhou, M.; Yan, J.; Wysocki, V. H. *Anal. Chem.* **2015**, *87*, 11879-11886.
(48) Muddiman, D. C.; Oberg, A. L. *Anal. Chem.* **2005**, *77*, 2406-2414.
(49) Goncalves, A. G.; Ducatti, D. R. B.; Grindley, T. B.; Duarte, M. E. R.; Noseda, M. D. *J. Am. Soc. Mass Spectrom.* **2010**, *21*, 1404-1416.
(50) la Marca, G.; Malvagia, S.; Toni, S.; Piccini, B.; Di Ciommo, V.; Bottazzo, G. F. *Nutr. Diabetes* **2013**, *3*, e94.
(51) Keki, S.; Nagy, L.; Deak, G.; Zsuga, M. *J. Am. Soc. Mass Spectrom.* **2005**, *16*, 152-157.
(52) Abraham, M. J.; Murtola, T.; Schulz, R.; Páll, S.; Smith, J. C.; Hess, B.; Lindahl, E. *SoftwareX* **2015**, *1–2*, 19-25.
(53) Pringle, S. D.; Giles, K.; Wildgoose, J. L.; Williams, J. P.; Slade, S. E.; Thalassinos, K.; Bateman, R. H.; Bowers, M. T.; Scrivens, J. H. *Int. J. Mass Spectrom.* **2007**, *261*, 1-12.
(54) Duez, Q.; Chirot, F.; Lienard, R.; Josse, T.; Choi, C.; Coulembier, O.; Dugourd, P.; Cornil, J.; Gerbaux, P.; De Winter, J. *J. Am. Soc. Mass Spectrom.* **2017**, *28*, 2483-2491.
(55) Van der Spoel, D.; Lindahl, E.; Hess, B.; Groenhof, G.; Mark, A. E.; Berendsen, H. J. C. *J. Comput. Chem.* **2005**, *26*, 1701-1718.
(56) Huang, J.; MacKerell, A. D. *J. Comput. Chem.* **2013**, *34*, 2135-2145.
(57) Abascal, J. L. F.; Vega, C. *J. Chem. Phys.* **2005**, *123*, 234505.
(58) Fischer, N. M.; van Maaren, P. J.; Ditz, J. C.; Yildirim, A.; van der Spoel, D. *J. Chem. Theor. Comp.* **2015**, *11*, 2938-2944.
(59) Mesleh, M. F.; Hunter, J. M.; Shvartsburg, A. A.; Schatz, G. C.; Jarrold, M. F. *J. Phys. Chem.* **1996**, *100*, 16082-16086.
(60) Ewing, S. A.; Donor, M. T.; Wilson, J. W.; Prell, J. S. *J. Am. Soc. Mass Spectrom.* **2017**, *28*, 587-596.
(61) Covey, T. R.; Thomson, B. A.; Schneider, B. B. *Mass Spectrom. Rev.* **2009**, *28*, 870-897.
(62) Abzalimov, R. R.; Kaltashov, I. A. *Anal. Chem.* **2010**, *82*, 7523–7526.
(63) Wang, R.; Zenobi, R. *J. Am. Soc. Mass Spectrom.* **2010**, *21*, 378-385.
(64) Liigand, P.; Heering, A.; Kaupmees, K.; Leito, I.; Girod, M.; Antoine, R.; Kruve, A. *J. Am. Soc. Mass Spectrom.* **2017**, *28*, 2124-2131.
(65) Gu, W.; Heil, P. E.; Choi, H.; Kim, K. *Appl. Phys. Lett.* **2007**, *91*, 064104.
(66) Laszlo, K. J.; Munger, E. B.; Bush, M. F. *J. Am. Chem. Soc.* **2016**, *138*, 9581-9588.
(67) Shelimov, K. B.; Clemmer, D. E.; Hudgins, R. R.; Jarrold, M. F. *J. Am. Chem. Soc.* **1997**, *119*, 2240-2248.

Figure Captions

Figure 1. ESI mass spectrum of PPG in aqueous solution (nominal average mass ~2000 Da; adjacent peaks correspond to ΔM = 58.04 Da). Three groups of signals arise from triply, doubly, and singly sodiated PPG. Highlighted peaks indicate the three charge states of PPG30 (*m/z* 609.40, 902.60, and 1782.21). PPG30 is one of the analytes studied in our MD simulations.

Figure 2. MD snapshots, representing different time points during the ESI process for (a) PPG10, (b) PPG30, and (c) PPG60 for droplets with an initial radius of 5.5 nm. In these MD runs PPG shows CEM-like behavior, i.e., ejection from the droplet surface). "IEM" (top right corner) highlights the ejection of a solvated Na^+. The final charge states of the PPG ions at t = 75 ns are indicated. Carbon atoms are shown in green, oxygens are red, Na^+ ions are shown as blue spheres.

Figure 3. (a) Example of a PPG10 simulation with an initial droplet radius of 5.5 nm. Ejection of a small progeny droplet carrying 2 Na^+ takes place at t = 1 ns; the fission line is shown in red. PPG10 is released into the gas phase via solvent evaporation to dryness. (b) Example of a simulation run during which PPG60 ejects from a 3 nm droplet via a two-tailed intermediate.

Figure 4. Droplet charge z_D relative to the Rayleigh charge z_R during ESI simulation runs, for initial radii of (a) 3 nm and (b) 5.5 nm. Shown in black, blue, and red are data for typical runs on droplets containing PPG10, PPG30, and PPG60. Gray lines represent predicted z_D / z_R profiles, calculated from eqs 1 and 2 for different values of z_D. Dashed lines highlight the z_D / z_R range between 0.8 and 1.0. The PPG60 data set ends at $n_{water} \approx 2000$ due to detachment from the droplet.

Figure 5. Summary of MD data for PPG10, PPG30, and PPG60. (a) - (c): Droplet radius 5.5 nm. (d) - (f): Droplet radius 3.0 nm. Each curve shows the number of water molecules in the droplet. Sudden drops to ~zero mark where PPG separated from the droplet. For each run the final PPG charge state and the number of waters at the detachment point is indicated; "n/a" marks instances where droplets evaporated to dryness without PPG detachment.

Figure 6. IMS analysis of various PPG ions. (a) singly sodiated PPG10. (b) - (d): PPG30 in charge states 1+ to 3+. (e) - (g): PPG60 in charge states 2+ to 4+. Each panel shows the measured Ω_{exp} distribution (black lines), as well as average Ω_{calc} values of the MD structures, taken from 1 μs vacuum simulation runs (red vertical lines). Horizontal red error bars represent the standard deviation of Ω_{calc}. Also included is a representative MD structure for each ion.

Figure 1

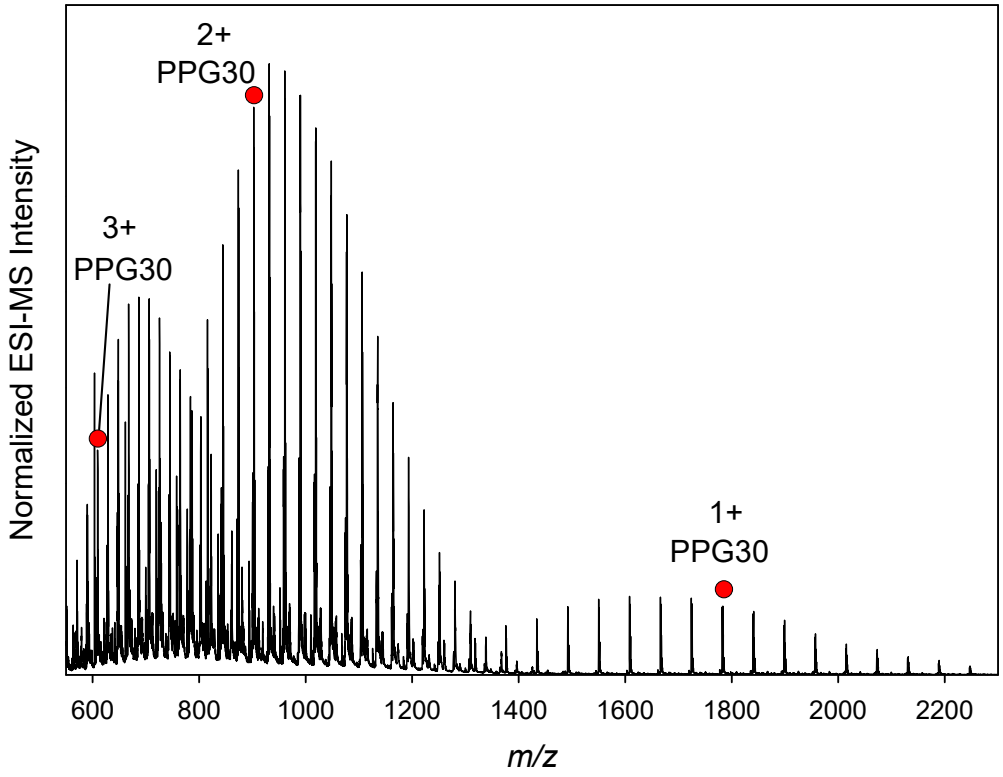
2+
PPG30
3+
PPG30
1+
PPG30
Normalized ESI-MS Intensity
600
800
1000
1200
1400
1600
1800
2000
2200
m/z

Figure 2

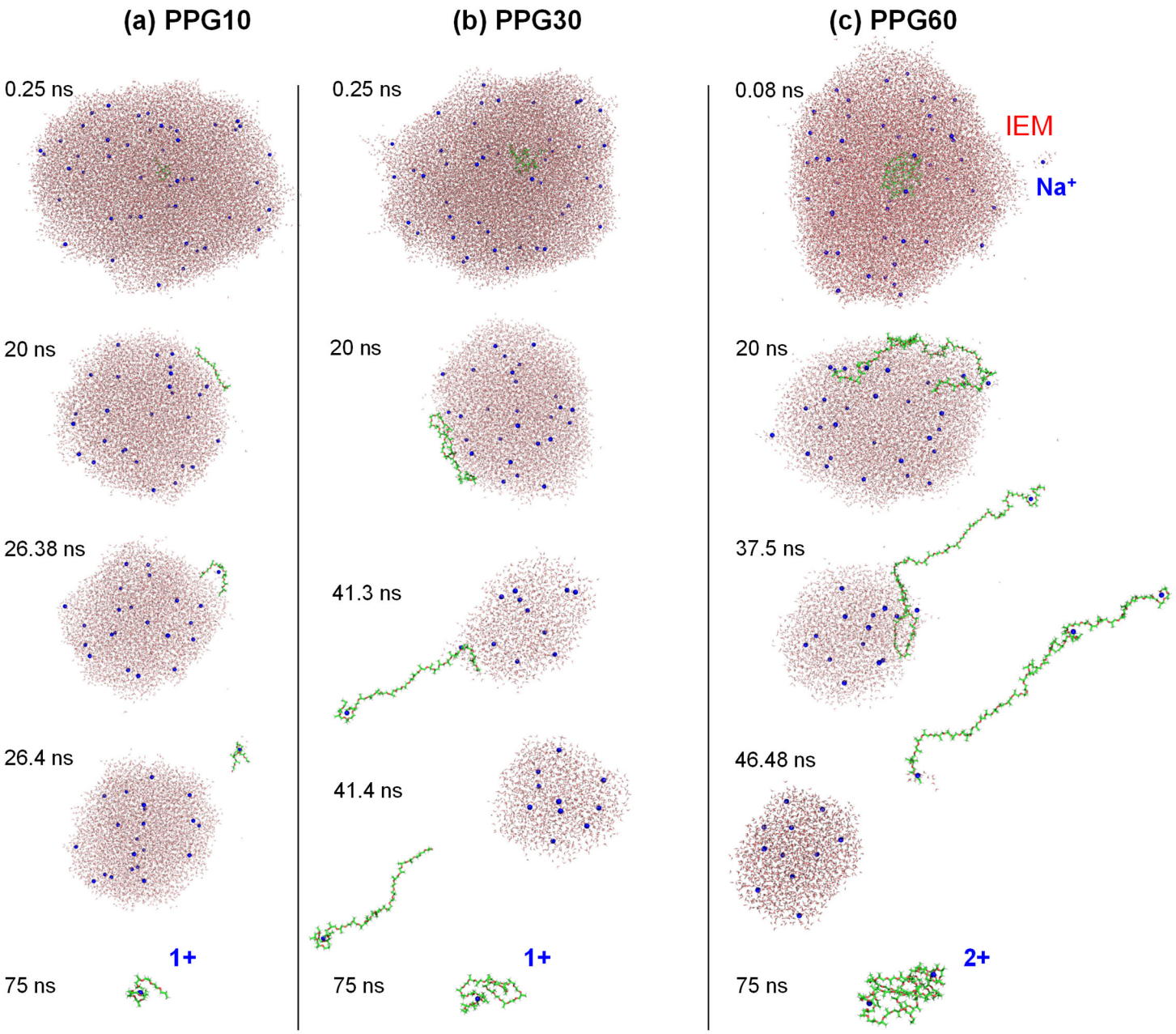
(a) PPG10
(b) PPG30
(c) PPG60
0.25 ns
20 ns
26.38 ns
26.4 ns
1+
75 ns
0.25 ns
20 ns
41.3 ns
41.4 ns
1+
75 ns
0.08 ns
IEM
Na+
20 ns
37.5 ns
46.48 ns
2+
75 ns

Figure 3

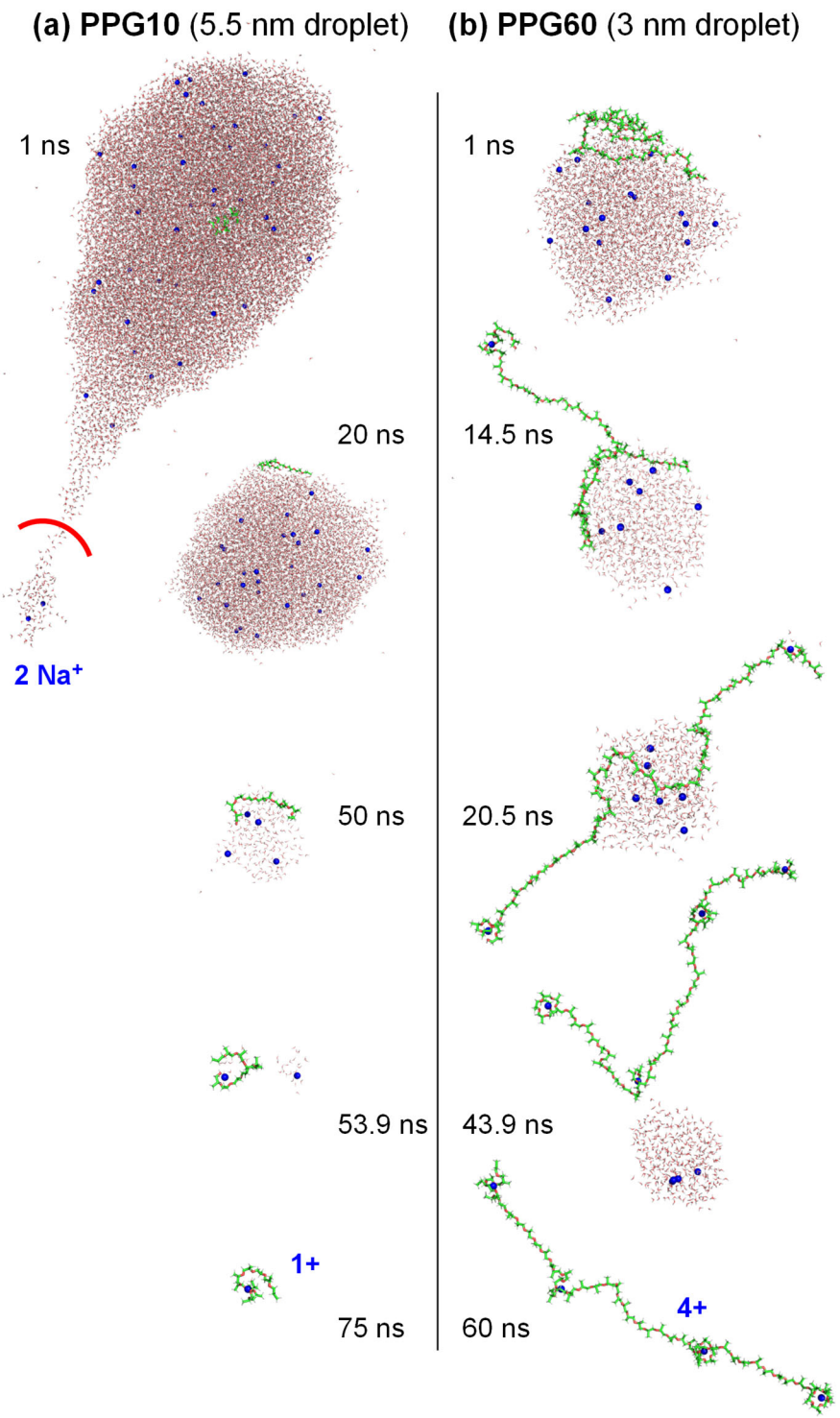
(a) PPG10 (5.5 nm droplet)
(b) PPG60 (3 nm droplet)
1 ns
20 ns
2 Na+
50 ns
53.9 ns
1+
75 ns
1 ns
14.5 ns
20.5 ns
43.9 ns
4+
60 ns

Figure 4

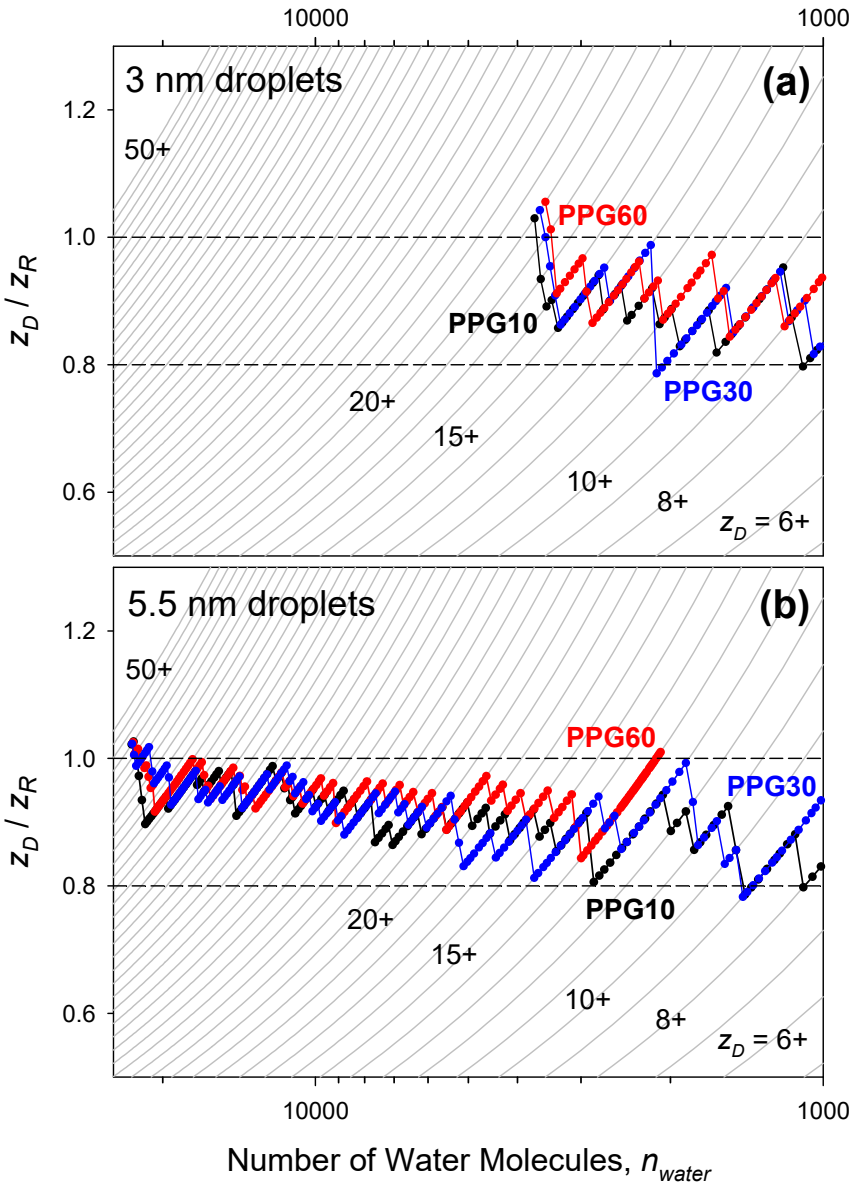
10000
1000
3 nm droplets
(a)
50+
PPG60
PPG10
PPG30
20+
15+
10+
8+
z_D = 6+
z_D / z_R
1.2
1.0
0.8
0.6
5.5 nm droplets
(b)
50+
PPG60
PPG30
PPG10
20+
15+
10+
8+
z_D = 6+
10000
1000
Number of Water Molecules, n_{water}

Figure 5

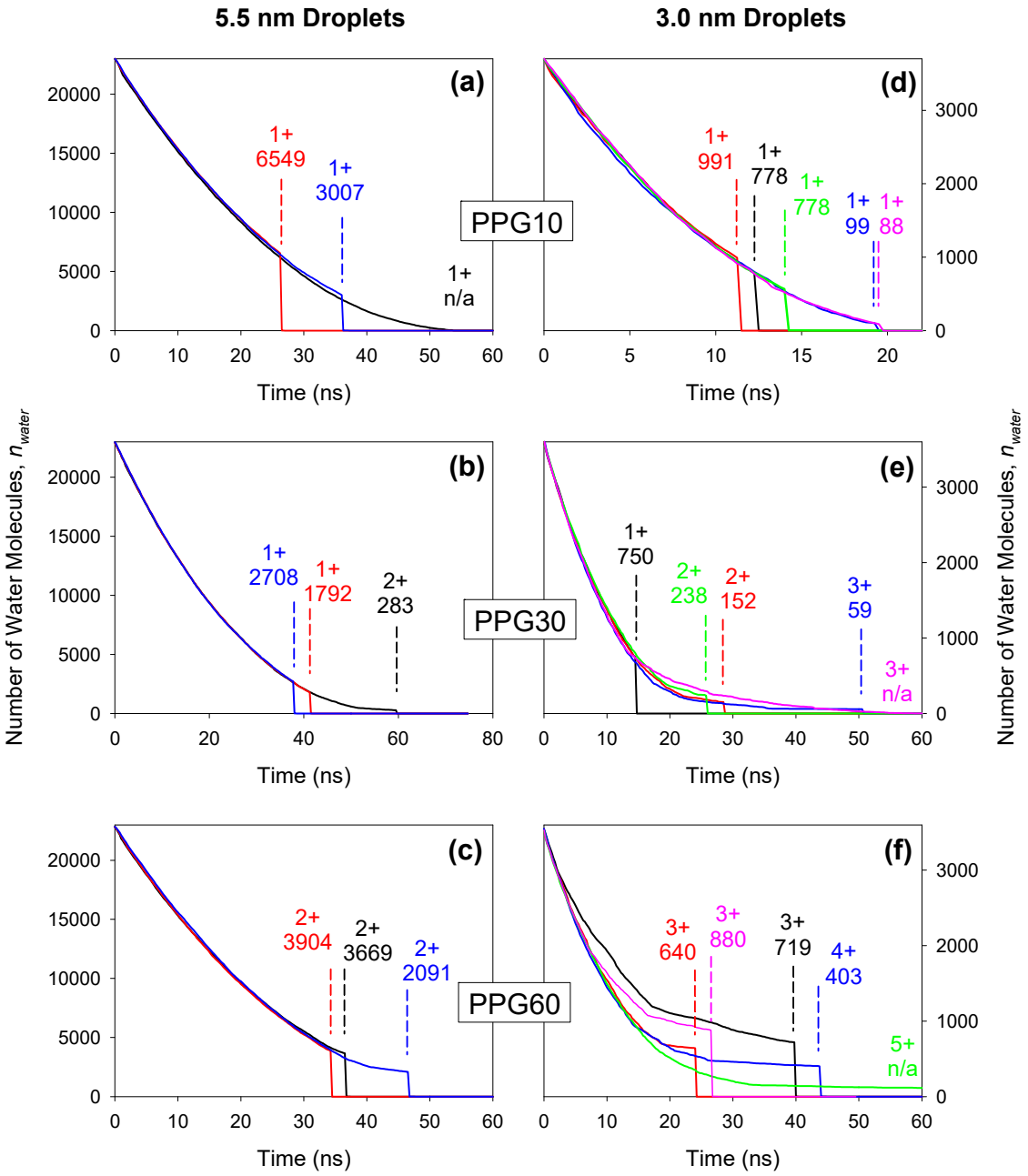
5.5 nm Droplets
3.0 nm Droplets
(a)
(b)
(c)
(d)
(e)
(f)
PPG10
PPG30
PPG60
1+ 6549
1+ 3007
1+ n/a
1+ 991
1+ 778
1+ 778
1+ 99
1+ 88
1+ 2708
1+ 1792
2+ 283
1+ 750
2+ 238
2+ 152
3+ 59
3+ n/a
2+ 3904
2+ 3669
2+ 2091
3+ 640
3+ 880
3+ 719
4+ 403
5+ n/a
Time (ns)
Number of Water Molecules, n_{water}

Figure 6

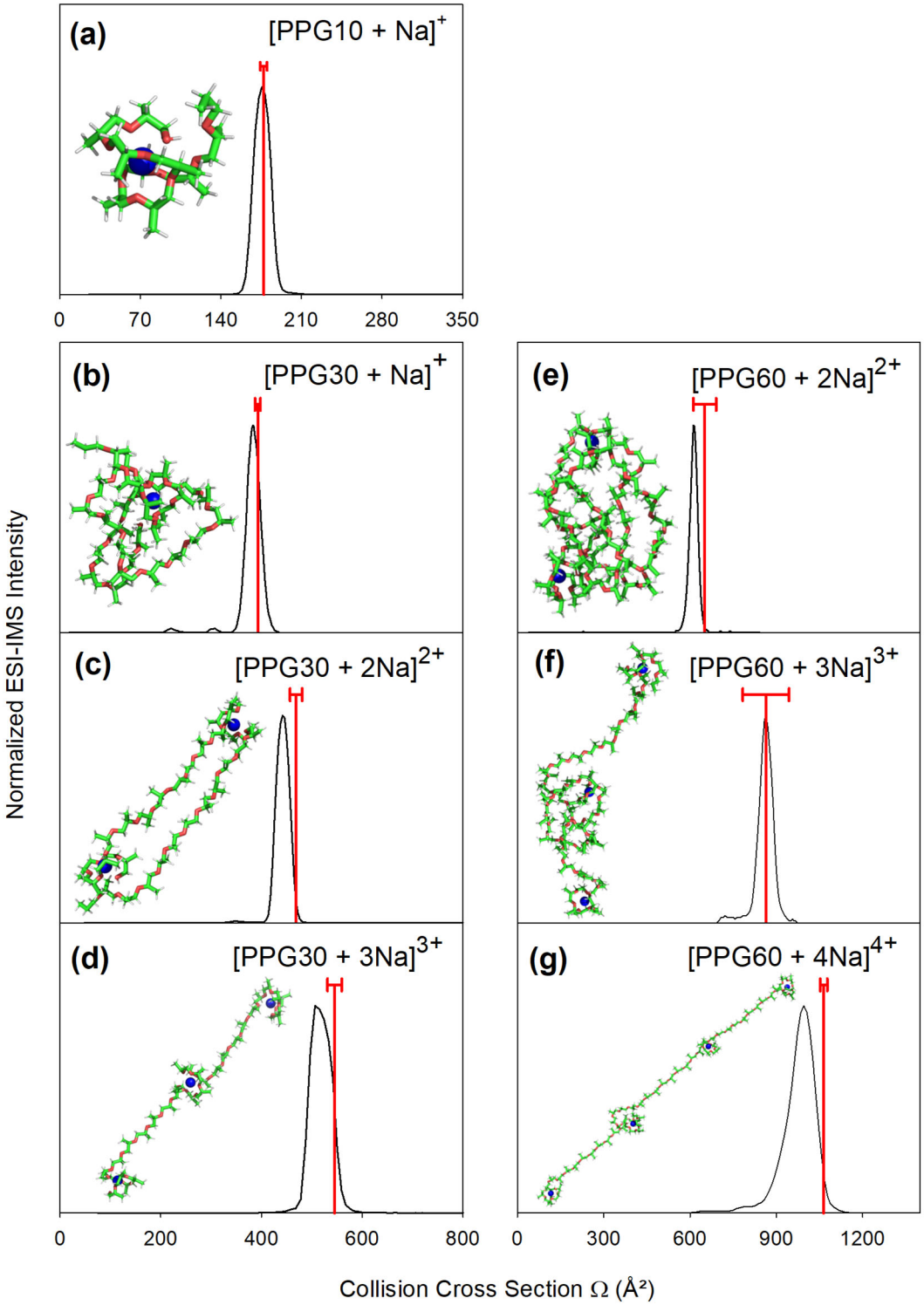
(a)
[PPG10 + Na]+
0
70
140
210
280
350
(b)
[PPG30 + Na]+
(c)
[PPG30 + 2Na]2+
(d)
[PPG30 + 3Na]3+
0
200
400
600
800
(e)
[PPG60 + 2Na]2+
(f)
[PPG60 + 3Na]3+
(g)
[PPG60 + 4Na]4+
0
300
600
900
1200
Normalized ESI-IMS Intensity
Collision Cross Section Ω (Å²)

For Table of Contents Only